

Unimolecular Submersible Nanomachines. Synthesis, Actuation, and Monitoring

Víctor García-López,[†] Pinn-Tsong Chiang,[†] Fang Chen,[‡] Gedeng Ruan,[†] Angel A. Martí,^{*,†} Anatoly B. Kolomeisky,^{*,†,§} Gufeng Wang,^{*,‡} and James M. Tour^{*,†,||}

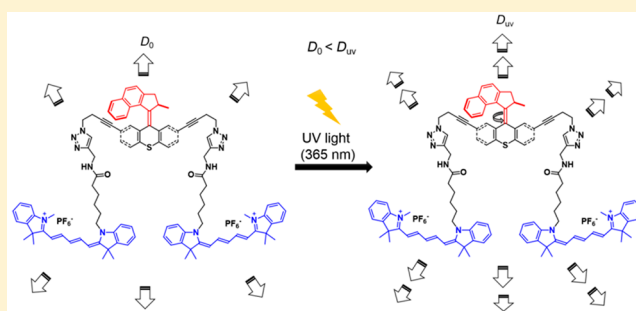
[†]Department of Chemistry, [§]Department of Chemical and Biomolecular Engineering and Center for Theoretical Biological Physics, ^{||}Department of Materials Science and NanoEngineering, Rice University, Houston, Texas 77005, United States

[‡]Department of Chemistry, North Carolina State University, Raleigh, North Carolina 27695, United States

S Supporting Information

ABSTRACT: Unimolecular submersible nanomachines (USNs) bearing light-driven motors and fluorophores are synthesized. NMR experiments demonstrate that the rotation of the motor is not quenched by the fluorophore and that the motor behaves in the same manner as the corresponding motor without attached fluorophores. No photo or thermal decomposition is observed. Through careful design of control molecules with no motor and with a slow motor, we found using single molecule fluorescence correlation spectroscopy that only the molecules with fast rotating speed (MHz range) show an enhancement in diffusion by 26% when the motor is fully activated by UV light. This suggests that the USN molecules give ~ 9 nm steps upon each motor actuation. A non-unidirectional rotating motor also results in a smaller, 10%, increase in diffusion. This study gives new insight into the light actuation of motorized molecules in solution.

KEYWORDS: Unimolecular submersible nanomachines, light-driven motor, diffusion coefficient, fluorophores



Inspired by the “bottom up” approach^{1–3} used by nature to build functional macroscopic entities using nanoscopic building blocks, synthetic chemists have designed a variety of molecular machines and nanovehicles such as nanoscale motors, switches, turnstiles, barrows, shuttles, and nanocars.⁴ Specifically, we have used scanning tunneling microscopy (STM)^{5–7} and single molecule fluorescence microscopy (SMFM)^{8–12} to track nanocars on surfaces. However, these imaging methods cannot be directly applied to unimolecular nanomachines in solution because they drift quickly out of focus in three-dimensional (3D) environments, thus producing trajectories that are too short to determine accurate diffusion coefficients.

As biological processes take place in solution, the development of nanomachines that are able to enhance their diffusion and perform work in that phase is of great interest. This has led to the development of self-propelled nanowires,^{13,14} micro-rockets,¹⁵ Janus-particle motors,^{16,17} enzymatic motors,^{18,19} and mineral micropumps²⁰ powered by chemical reactions through self-electrophoretic mechanisms, bubble propulsion, or diffusiophoresis. However, most of those micromachines use or generate toxic chemicals that are inappropriate for in vivo applications. To address the disadvantage of using toxic chemicals, cleaner systems that convert photonic energy to translational motion have been developed. Silver chloride particles²¹ and TiO₂ micromotors^{22,23} are some examples of

micromachines able to move in solution under UV light illumination via a self-diffusiophoresis mechanism.

All of the micromachines mentioned above range from hundreds of nanometers to micrometers in size. At present, there are only two examples of catalytically driven unimolecular nanomachines (<10 nm in size) reported in the literature.^{24,25} These unimolecular motors consist of a ruthenium-based Grubbs’s catalyst and are powered by a ring-opening or a ring-closing metathesis polymerization. Though there are many examples of synthetic light-driven rotary molecular motors, particularly as developed by Feringa,^{26–28} their potential to promote solution-phase locomotion at the molecular scale remains unreported. Therefore, the development of truly molecular-sized light-driven nanomachines capable of directed motion, or promoted diffusion over a relatively long time scale (microseconds) in solution has not been reported. The main hurdle in the development of actuated unimolecular nanomachines is the smallness in size of the propelled entity. At this scale, not only are monitoring and tracking difficult tasks, but the influence of Brownian motion can be overwhelming.

Microscopic and even nanoscopic “swimmers,” residing in the domain of ultralow Reynolds numbers, have been

Received: September 17, 2015

Revised: October 30, 2015

Published: November 5, 2015

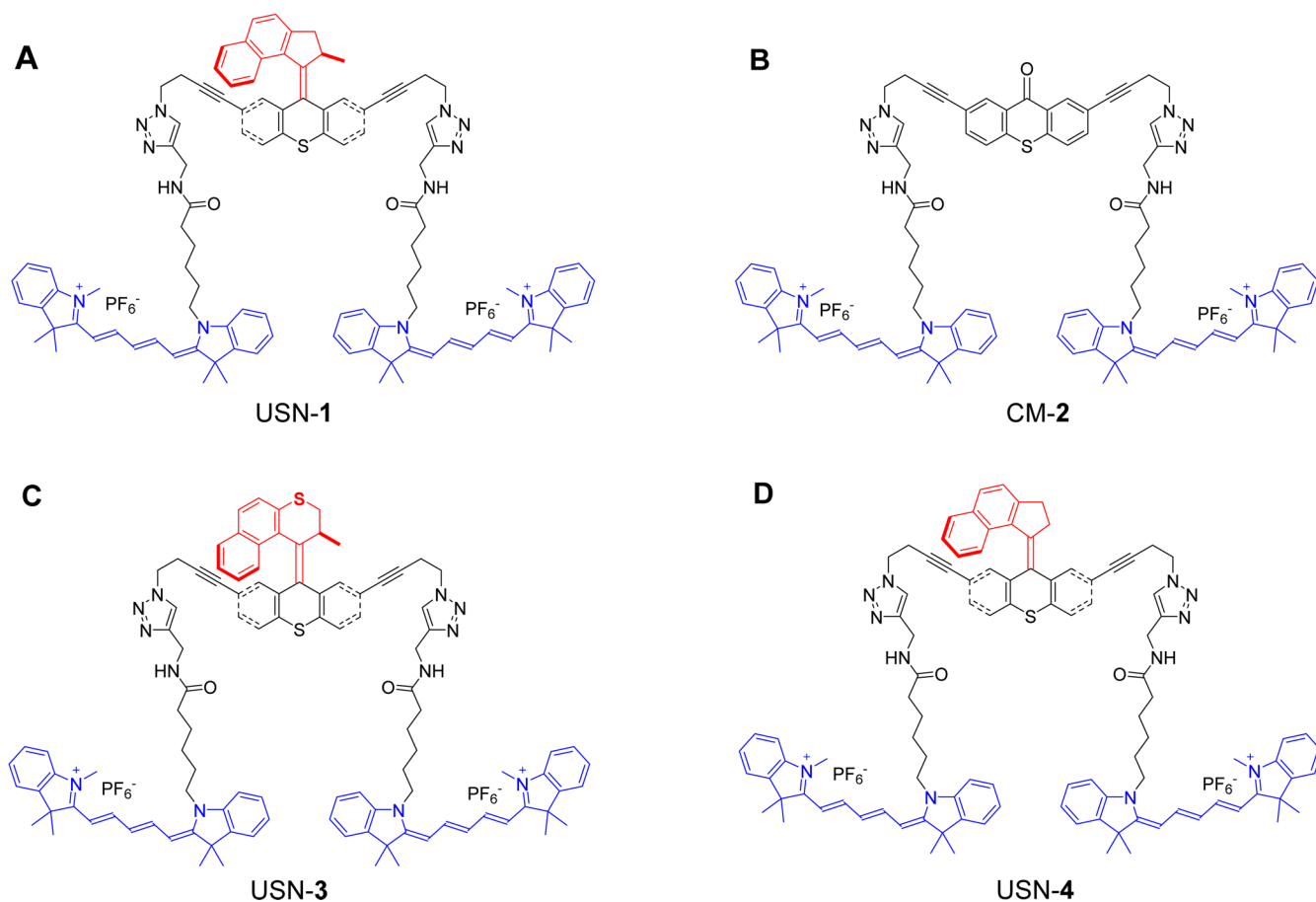


Figure 1. USNs and a control molecule. (a) USN-1 with a 2–3 MHz unidirectional rotating motor;²⁶ (b) control molecule CM-2 without a rotor; (c) USN-3 with a slow motor which operates at 2 rotations per hour;^{27,39} and (d) USN-4 with a non-unidirectional preference for motor rotation. The rotor portions are shown in red, the stator portions in black, and the fluorophores (part of the stator) in blue. In this and the following figures and schemes, the four structures are drawn in conformations to underscore the motor operation. However, in reality, they will certainly have many randomly oriented conformations in solution.

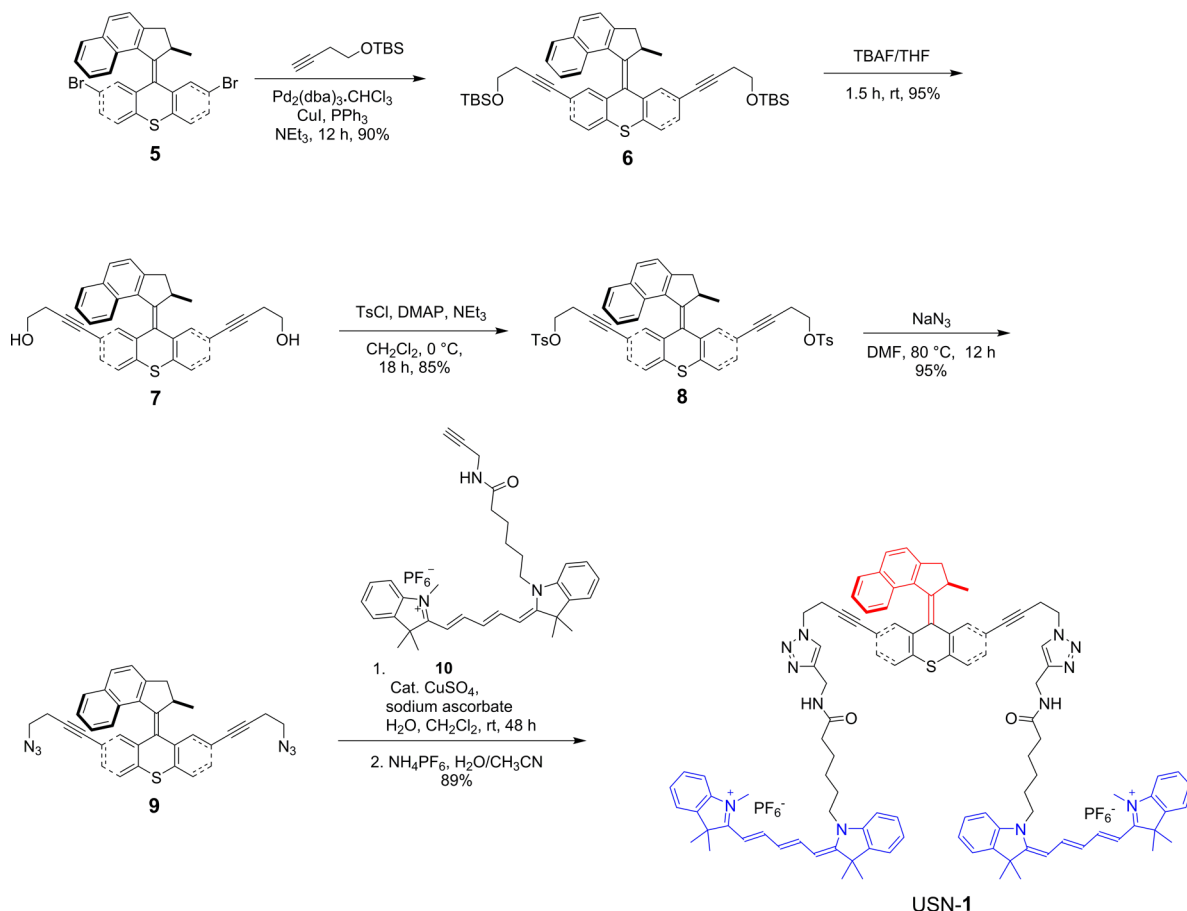
extensively studied by theorists: in the 1950s (Taylor²⁹ and Ludwig³⁰) through the 1970s and 1980s (Purcell³¹ and Brenner^{32,33}) and more recently (Nelson, Zhang, Peyer^{34–36} and Powers³⁷); the results are now summarized in a recent book.³⁸ Since inertia has no influence at these scales, macroscale swimming dynamics are inapplicable. Movement is generally accomplished by mitigating time reversibility and escaping from the so-called “scallop” effect. Actuated diffusional increases of molecular-sized entities are predicted to be possible by some mechanical mechanisms, such as propagation of sinusoidal traveling waves along the small-sized body, or by screw-like or flexible oar-like movements.³⁸

In this study, we used single molecule fluorescence correlation spectroscopy (FCS) to monitor promoted motion of single-molecule nanomachines in solutions when being activated by UV light. As we shall see in the later discussion, in free solution, the movement of single nanomachine molecules is always under the influence of rotational and translational Brownian motions. For example, the molecule can diffuse ~17 nm within the shortest time between two motor actuation events (~500 ns), assuming the nanomachine molecule has a diffusion coefficient of $10^{-10} \text{ m}^2 \cdot \text{s}^{-1}$. However, when we excited the motor at a rate approaching its maximum cycling speed, we observed that the apparent diffusion coefficient significantly increased, indicating a directed motion, at least for some periods of time, when the molecular machines were activated

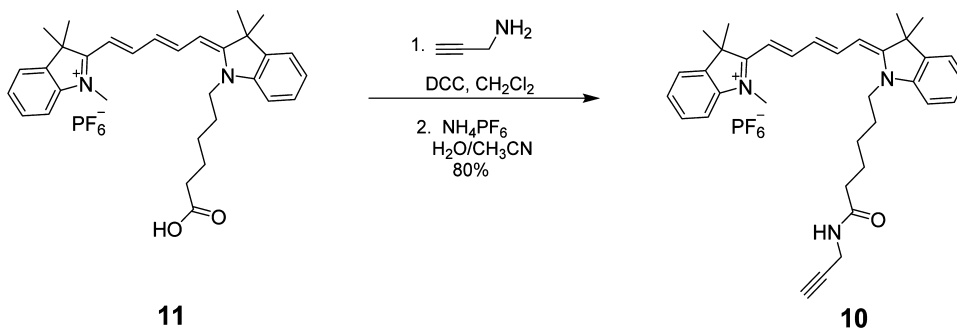
by light. These molecules bear unidirectional rotating motors and fluorophores for optical tracking. We name these systems unimolecular submersible nanomachines (USNs). The design includes a light-driven motor functionalized at the stator with aliphatic chains that work as spacers between the motor and the fluorophores (Figure 1). But when the molecular motors are activated by UV light, USN-1 showed expedited diffusion by a factor of 1.26 (26%). We carefully designed and studied the diffusion of control molecules with no rotor (CM-2), a slow motor (USN-3),^{27,39} or a non-unidirectional rotating motor (USN-4). We found that a fast rotating motor with its 2–3 MHz²⁶ rotational rate is critical for enhanced UV light-activated diffusion, while the non-unidirectional spinning motor (USN-4) also shows enhanced diffusion, albeit smaller. The enhancement of 26% in diffusion suggests that upon each motor actuation, the USN molecules will give a ~9 nm step, a length several times larger than its molecular size! The mechanism by which motor actuation drives the molecule in solution is still under study, but our results give new insight into the design of solution-based motorized nanomachines.

Results and Discussion. The synthesis of USN-1 started with a Sonogashira coupling between **5**⁷ and 4-(*tert*-butyldimethylsilyoxy)but-1-yne to afford **6**. Removal of the *tert*-butyldimethylsilyoxy (TBS) group was completed using tetrabutylammonium fluoride (TBAF) to form **7**. Diol **7** was ditosylated to afford **8** in good yield. Azide motor **9** was

Scheme 1. Key Portions of the Synthesis of USN-1



Scheme 2. Synthesis of cy5 10



synthesized in high yield by a substitution reaction between **8** and sodium azide. The final step of the synthesis is a double azide–alkyne Huisgen cycloaddition between azide **9** and cy5 derivative **10** followed by ion exchange to afford USN-1 (Schemes 1 and 2). The entire synthesis was 20 steps, but only the key portions are shown. The syntheses of CM-2, USN-3, and USN-4 were performed following the same synthetic approach starting from the corresponding 2,7-dibromomotor or 2,7-dibromothioxanthene (Schemes 3, 4, and 5).

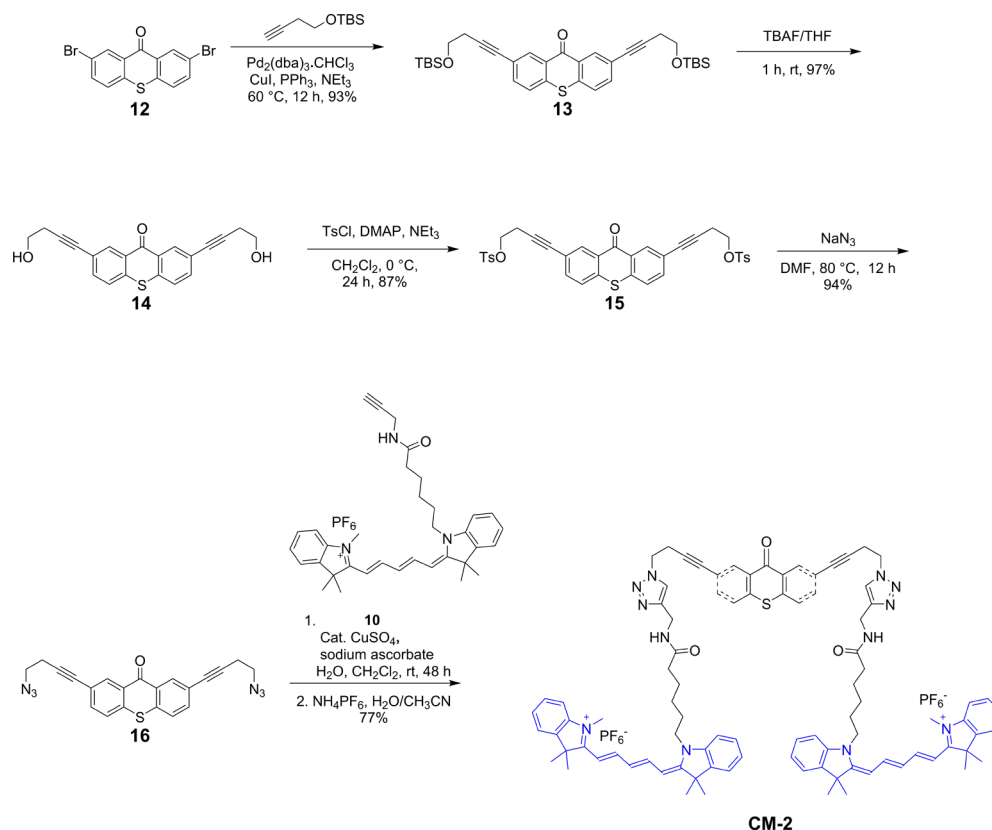
Cy5 was chosen as a fluorophore for two reasons: it has near zero absorption at the 350–370 nm activation region of the motor and its maximum absorption region (640 nm) is optically well-separated from the activation region of the motor, minimizing the possibility of energy transfer (Figure 2).

To verify that no quenching of the motor was induced by the cy5, half of the rotation of the slow motor without cy5 (**32**) and

with cy5 (USN-3) was monitored by ^1H NMR (Figure 3). Due its fast rotation, USN-1 cannot be monitored by NMR. After 1 h of UV irradiation, the unstable isomer was formed with 88% yield for motor **32** and 86% yield for USN-3. This demonstrates that the cy5 does not interfere with the photoisomerization of the motor. Then, the samples were heated at 60 $^\circ\text{C}$ for 1 h to facilitate the thermal helix inversion and to obtain the stable isomers. The chemical shifts returned to the original values indicating that no photo or thermal decomposition occurs during UV irradiation and heating.

To study the natural and activated diffusion of the USNs in acetonitrile (ACN), a home-built confocal fluorescence microscope system was used (Supporting Information Figure S1).⁴⁰ The cy5 dye excitation was performed at 633 nm, and for the motor activation a UV LED emitting at 365 nm was used. In single molecule FCS experiments, determination of the

Scheme 3. Synthesis of CM-2



absolute diffusion coefficient of molecules depends on experimentally adjustable parameters such as laser beam waist-size. Such parameters may vary slightly from time to time, introducing errors to the measurements.⁴¹ To minimize these systematic errors, the FCS experiments with and without UV excitation were always collected in pairs using the same solution and at the same collection spot. Hence, the only contrast was with or without UV light illumination. The sequence of collection has no observable effect on the diffusion coefficient measurements.

In the absence of UV light activation, USN-1 diffuses freely in bulk solutions. The autocorrelation function (ACF) can be satisfactorily fitted with the 3D diffusion model (Figures S2 and S3). The diffusion coefficient (D) of USN-1 was $0.92 \pm 0.07 \times 10^{-10} \text{ m}^2 \cdot \text{s}^{-1}$ (95% confidence interval from Student's t test) from repeated measurements on different days and for different samples. This D is on the same order of magnitude for other small molecules in ACN.⁴²

When the UV light was turned on, the diffusion of USN-1 becomes faster. This can be viewed from the ACF decays. Figure 4A shows the normalized ACFs of 20 measurements each in the absence and the presence of UV light. It is apparent that the ACFs are bundled into two groups, with the ACFs in the presence of UV light decaying faster, indicating a faster diffusion. Figure 4B displays the recovered D distributions, which shows that the D s of USN-1 in the presence of UV light are significantly larger than those in the absence of UV light. The mean and 95% confidence intervals are reported in Table 1. The diffusion coefficient was enhanced by a factor of 1.26 (26%). A Student's t test shows that with a confidence level >99.95%, the diffusions in the presence and absence of UV excitation are different.

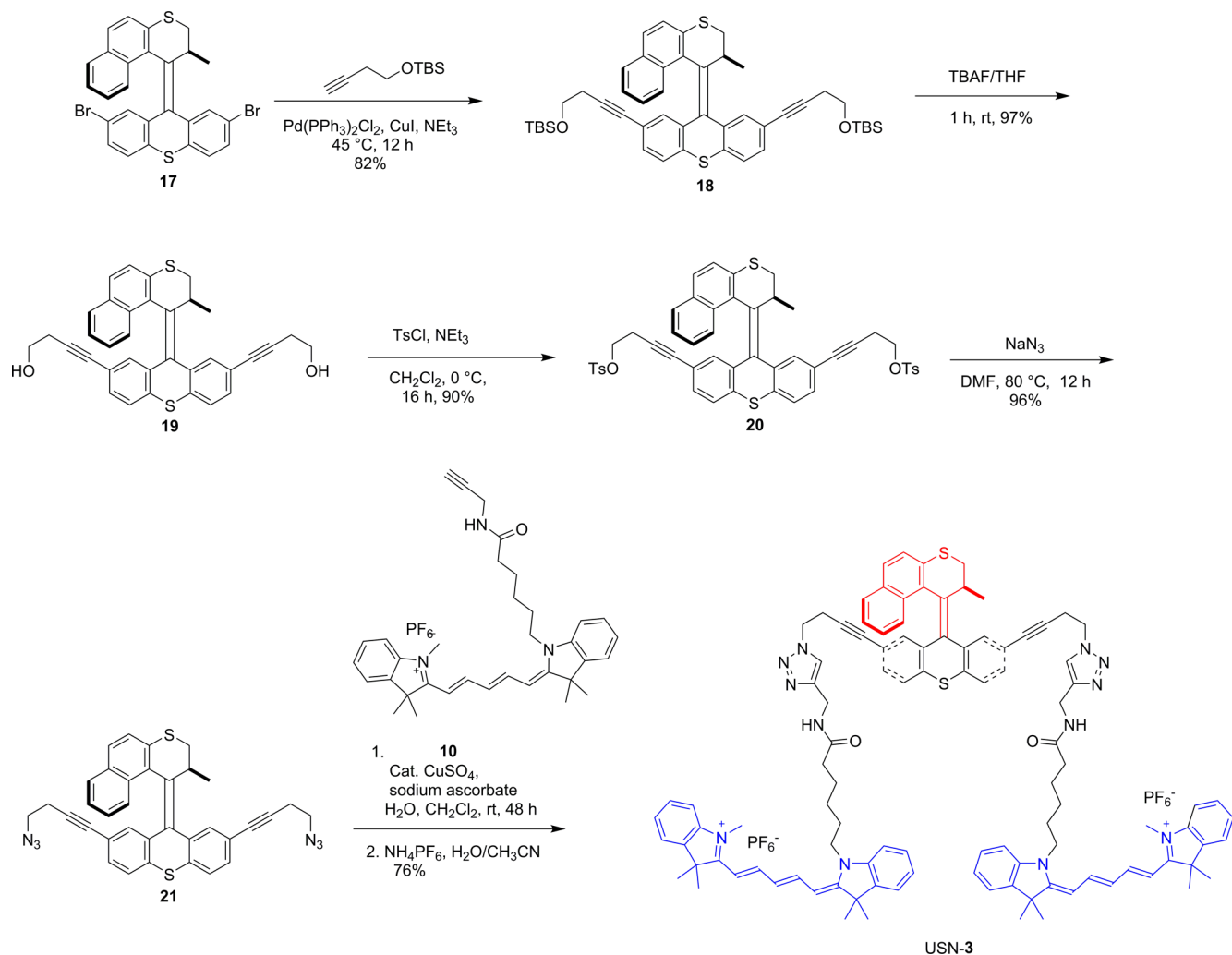
As a contrast, we also measured the D of a control molecule, CM-2, in the presence and absence of UV light. The only difference between USN-1 and CM-2 is that there is no rotor moiety in CM-2. Figure 4C,D shows the corresponding ACFs and their recovered D distributions, respectively. The two bundles of ACFs completely overlap, indicating that there is no observable diffusional difference with or without UV light activation. The recovered D of CM-2 shows a similar D in ACN than USN-1 (Table 1). The lack of difference in the recovered D s of CM-2 indicates that UV light does not increase the diffusion of that rotorless control molecule.

To further study the relationship between the enhanced molecular diffusion and the motor activation, we studied two USNs with varied structures. USN-3 has a motor with a six-membered ring, reducing the rotation speed to ~ 2 revolutions per hour.^{27,39} Figure 4E,F shows the observed ACFs and diffusion coefficient distributions in the presence and absence of the UV excitation. Therefore, no enhanced diffusion was observed when the motor is rotating at slow speed.

USN-4 is designed without the methyl group as seen in USN-1. This structural change causes the loss of unidirectionality, and subsequently the rotor randomly inverts its rotational direction. As shown in Figure 4G,H, the mean of the diffusion coefficients of UV-activated USN-4 was marginally enhanced by a factor of 1.10 (10%). A Student's t test confidence level is >99.8%, suggesting that the diffusion of USN-4 is enhanced in the presence of UV activation.

The smaller enhancement in the diffusion of USN-4 could result from two possible reasons: (1) the step size of the molecule is smaller or (2) the rotation speed is slower. The rate at which the nondirectional rotor in USN-4 moves is unknown. We know that if the stereogenic center-appended methyl

Scheme 4. Key Portions of the Synthesis of USN-3



substituent in USN-1 is replaced by a *tert*-butyl group, the motor is reported to have an increased rotational rate from 2 to 3 MHz to >150 MHz.⁴³ Increasing the steric bulk from methyl to *tert*-butyl likely raises the energy of the intermediate needed for the thermal helix inversion step, making the helix inversion more facile. Likewise, going from the methyl group in USN-1 to the smaller proton in USN-4 will likely lower the energy of the intermediate in USN-4, slowing its rotation. This could account for the slowing of USN-4 relative to USN-1, rather than any effect of unidirectionality vs nondirectional rotation of the rotor.

The enhanced diffusion is not caused by the local heating effect of the excitation laser or the UV light. First, both USN-3 and CM-2 serve as excellent control molecules since they have a similar mother-ring structure and the same amount of fluorophores (cy5) as USN-1. However, their diffusion does not increase with UV excitation. Second, we further designed control experiments to exclude the possibility of a heating effect. There are three possible sources for the heating effect: (1) solvent absorption of the excitation laser; (2) fluorophore absorption of the excitation laser; and (3) motor absorption of the UV light.

(1) The heating effect caused by the solvent absorption of the excitation laser. It has been well-documented and generally accepted that a mW level laser beam will not cause significant

temperature change in the solvent due to solvent absorption; this has been extensively studied by Hell.⁴⁴

(2) The heating effect caused by the fluorophore absorption of the 633 nm laser. It is generally accepted in single molecule FCS that the heating caused by fluorophore absorption at the 1.0 mW laser excitation level has a negligible effect upon diffusion. We further confirmed this by varying the 633 nm excitation laser power by a factor of 2.5 (1.2 mW). Note the window for the excitation laser power is very narrow as too much laser power photobleaches the molecules, we do not obtain sufficient signal for too low laser power.⁴⁵ The corresponding ACF curves and their statistical analyses are shown in Figure S4. The recovered diffusion coefficients using a 3D diffusion model are $0.91 \pm 0.11 (\times 10^{-10} \text{ m}^2 \cdot \text{s}^{-1})$ and $0.93 \pm 0.10 (\times 10^{-10} \text{ m}^2 \cdot \text{s}^{-1})$ for the 3.0 and 1.2 mW excitation laser powers, respectively. Overlapping of the corresponding ACF curves and their statistical analyses shows that there is no significant difference in diffusion, indicating that there is negligible local heating effect from the 633 nm laser.

(3) The heating effect caused by motor absorption of the UV light. The UV light power ($10 \text{ kW}/\text{cm}^2$) is 2 orders of magnitude smaller than that of the 633 nm laser ($3.0 \text{ MW}/\text{cm}^2$). It is reasonable to infer that the heating caused by the absorption of the UV light is also negligible. However, we noticed that there is a small difference in the UV-vis spectra

Scheme 5. Synthesis of USN-4

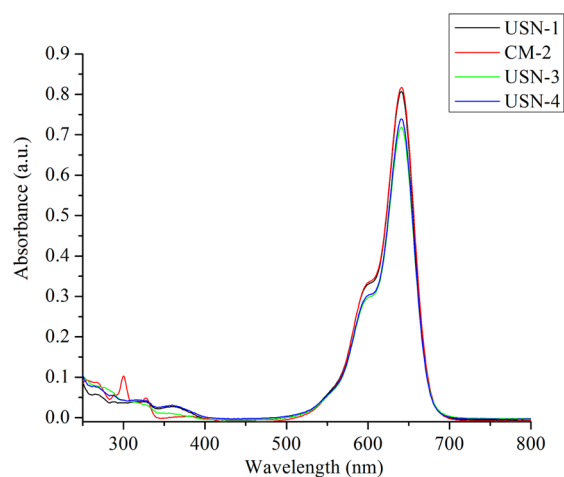
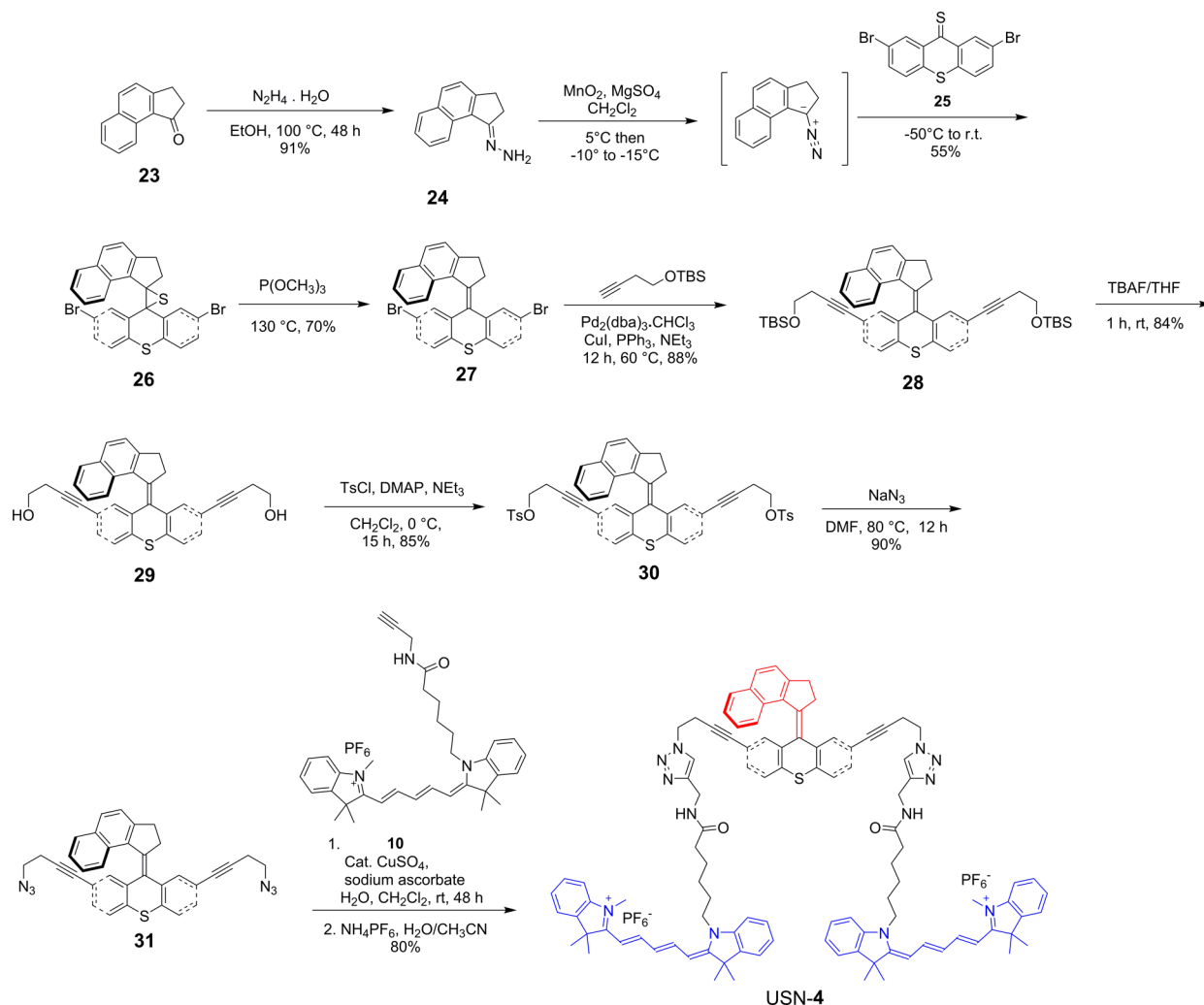


Figure 2. Absorption spectra of USN-1, CM-2, USN-3, and USN-4 in ACN.

for USN-1 and its control molecules (Figures S5–S8 and Table S1). Interestingly, the molar absorptivity of the fast rotating motors: USN-1 and USN-4 at 360 nm ($15,400$ and $14,700$ $\text{M}^{-1} \text{cm}^{-1}$, respectively) are larger than those of CM-2 and USN-3 (6400 and 7500 $\text{M}^{-1} \text{cm}^{-1}$, respectively). It is likely that this difference in UV absorption is related to the excitation and

subsequent rotation of the motors. To further exclude the possibility of the heating effect of the UV light due to this difference in molar absorptivity, we did another control experiment using a previously synthesized nanocar 33. Nanocar 33 has four adamantane wheels and two BODIPY dyes¹² whose extinction coefficient is $64,900$ $\text{M}^{-1} \text{cm}^{-1}$ at 360 nm (Figure S9). The diffusion coefficient of nanocar 33 was measured in the presence and absence of the UV light illumination on the same confocal fluorescence microscope with a 514 nm laser excitation (0.3 mW or 0.5 MW/cm²). The corresponding ACF curves and their nonlinear least-squares (NLLS) analyses are shown in Figure S10. The recovered diffusion coefficients are 1.11 ± 0.04 ($\times 10^{-10}$ $\text{m}^2 \cdot \text{s}^{-1}$) and 1.10 ± 0.05 ($\times 10^{-10}$ $\text{m}^2 \cdot \text{s}^{-1}$) in the absence and presence of the UV light, respectively. There is no significant difference in diffusion, indicating that the heating effect due to the absorption of the UV light is negligible even for molecules with an absorption coefficient $4\times$ larger at 360 nm. Based on these arguments, we conclude that the observed enhanced diffusion is not due to the heating effect of the excitation UV light or the laser beam. The enhanced diffusion is due to the motor actuation by UV light.

The enhanced diffusion for USN-1 and USN-4 molecules can only be observed when the UV photon flux is sufficiently high as our early attempts using low illumination power all failed. At the specified excitation level, the molecule should

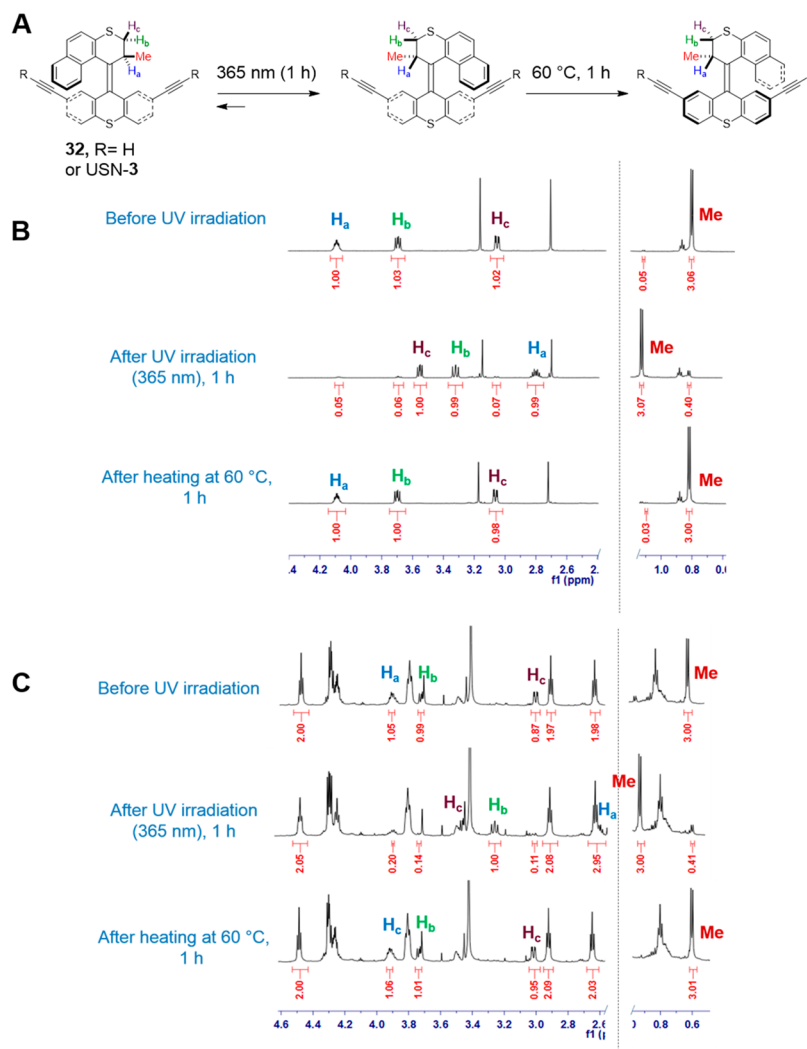


Figure 3. Partial ¹H NMR (CD₃CN) spectra of half-rotation of the slow motor in 32 and USN-3. (A) Schematic representation of half rotation of the slow motor. (B) Partial ¹H NMR spectra of half-rotation of slow motor 32 showing 88% photoisomerization conversion and 99% thermal helix inversion. (C) Partial ¹H NMR spectra half-rotation of USN-3 showing 86% photoisomerization conversion and 99% thermal helix inversion. The yields of the conversion were calculated using the integration values of the methyl group (Me).

diffuse by a distance $L \sim 17$ nm in the 3D space between two motor actuation events (~ 500 ns) according to Einstein eq 1 ($D \sim 1 \times 10^{-10}$ m²·s⁻¹):

$$L^2 = 2nD_0t \quad (1)$$

where L^2 is the mean square displacement; n is number of dimensions; D_0 is the diffusion coefficient; and t is time interval between two motor excitations. When the UV excitation is close to or over the motor saturation level, t can be approximated as the limiting cycle time of the motor. Under UV activation, eq 1 becomes

$$L^2 + r^2 = 2nD't \quad (2)$$

where r is the displacement of the USN after each actuation; D' is the apparent diffusion coefficient. Note that, r is randomly oriented with respect to L . Thus, an increased D' by 1.26 times indicates that r , the displacement of the nanomachine under each motor stroke, is ~ 8.6 nm, a length several times larger than its molecular size!

To investigate how the motor responds to UV light in viscous environments, the diffusion of USNs in a more viscous solution was also investigated. A viscous solvent, 2,2'-

thiodiethanol (TDE, S(CH₂CH₂OH)₂) was used to mix with ACN to form a binary mixture. 10% of TDE was added so the dynamic viscosity of the solvent was nearly doubled (1.9×), while the viscosity was still low (0.65 mPa s). The diffusion coefficient of USN-1 becomes smaller in the viscous solvent by a factor of 1.7 (Table 2 and Figure S), qualitatively consistent with Einstein–Stokes equation:

$$D = \frac{k_B T}{6\pi\eta R_m} \quad (3)$$

while USN-1 diffusion was enhanced when the UV excitation was turned on in the viscous solvent, the ratio of the enhancement in the diffusion is approximately constant. As the relative viscosity increased by a factor of 1.9, the diffusion enhancement only changed from 1.26 to 1.23. This shows that the viscosity of the solvent will not significantly affect the diffusion enhancement.

In conclusion, we observed that USNs bearing fast light-driven motors show increased diffusion in the solution phase when the motor is activated by UV light. We demonstrated that the motor rotation is not affected by the fluorophores. Through

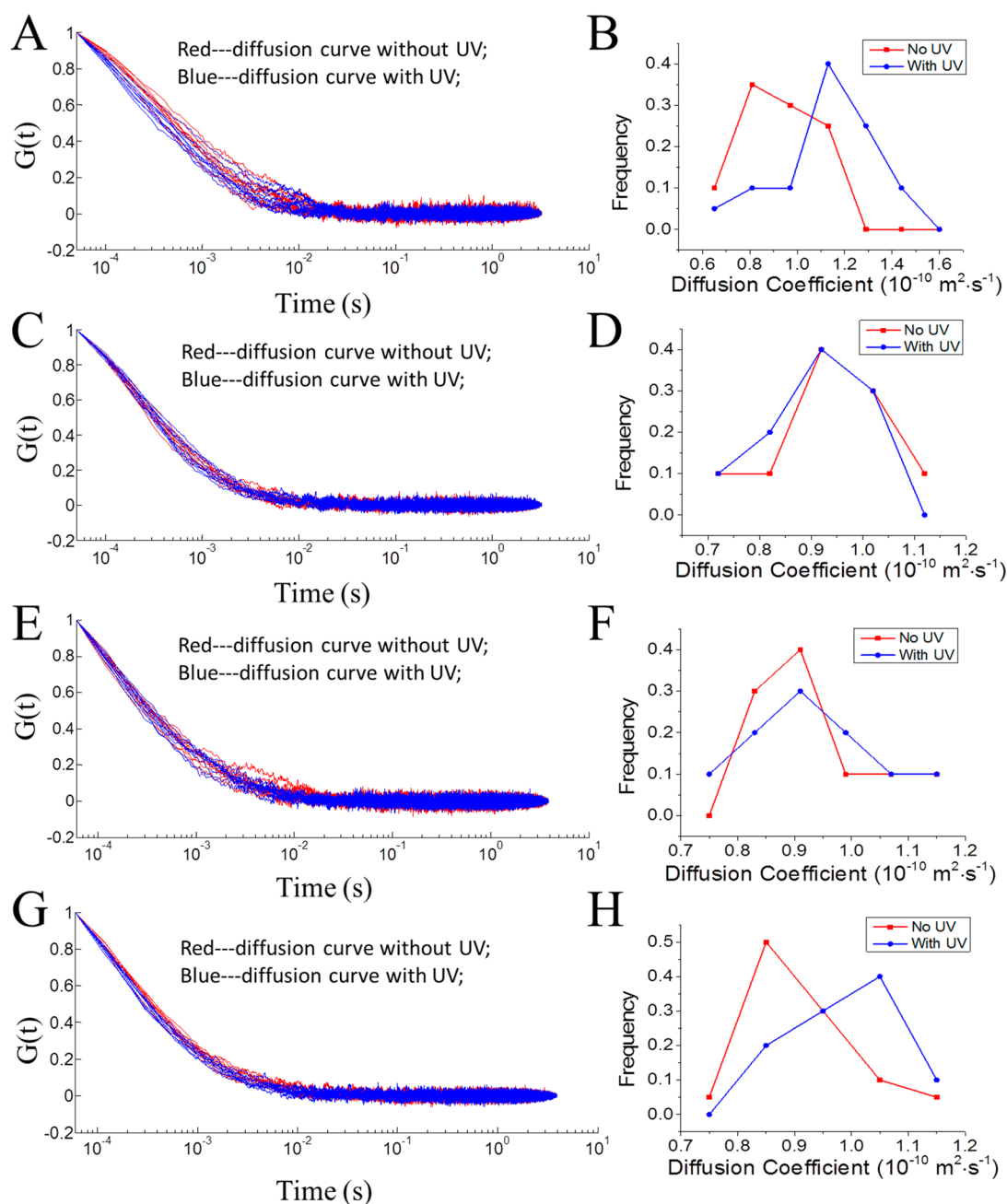


Figure 4. Comparison of diffusion coefficients of USNs in ACN in the presence and absence of UV light activation. (A, B) USN-1; (C, D) CM-2; (E, F) USN-3; and (G, H) USN-4. (A, C, E, G) are the normalized ACFs of 20 measurements each in the presence and absence of UV light. Red: without UV activation. Blue curves: with UV. (B, D, F, H) are the histograms of recovered diffusion coefficient using nonlinear least-squares fitting from the ACFs. For USN-1 and USN-4, the ACFs are bundled into separate groups in the presence and absence of the UV light, respectively, indicating their diffusion behaviors are significantly different with or without UV light illumination. Using NLLS fitting, the recovered diffusion coefficient D s of USN-1 and USN-4 in the presence of UV light are significantly larger than those in the absence of UV light (Table 1). The UV light was provided by a gallium indium nitride 365 nm UV LED with an intensity of ~ 10 mW. The UV light was optically filtered and tightly focused by a high numerical aperture objective (NA 1.4) to a spot with an estimated diameter of $\sim 10 \mu\text{m}$. The excitation level was $\sim 1.0 \times 10^4 \text{ W cm}^{-2}$.

Table 1. Apparent Diffusion Coefficients of the USN Series in the Absence and Presence of UV Light Activation^a

	D (no activation) ($\times 10^{-10} \text{ m}^2 \cdot \text{s}^{-1}$)	D (UV activation) ($\times 10^{-10} \text{ m}^2 \cdot \text{s}^{-1}$)	diffusion coefficient ratio
USN-1	0.92 ± 0.07	1.16 ± 0.10	1.26
CM-2	0.92 ± 0.07	0.93 ± 0.06	1.01
USN-3	0.90 ± 0.06	0.93 ± 0.08	1.03
USN-4	0.89 ± 0.04	0.98 ± 0.04	1.10

^aThe diffusion coefficients are reported with 95% confidence intervals using Student's t -test.

Table 2. Apparent Diffusion Coefficients of USN-1 in Viscous Solutions in the Absence and Presence of UV Light Activation^a

TDE %	viscosity (mPa·s)	D (no activation) ($\times 10^{-10} \text{ m}^2\cdot\text{s}^{-1}$)	D (UV activation) ($\times 10^{-10} \text{ m}^2\cdot\text{s}^{-1}$)	diffusion enhancement
0	0.34	0.92 ± 0.07	1.16 ± 0.10	1.26
10	0.65	0.53 ± 0.02	0.65 ± 0.01	1.23

^aThe diffusion coefficients are reported with 95% confidence intervals using Student's t -test.

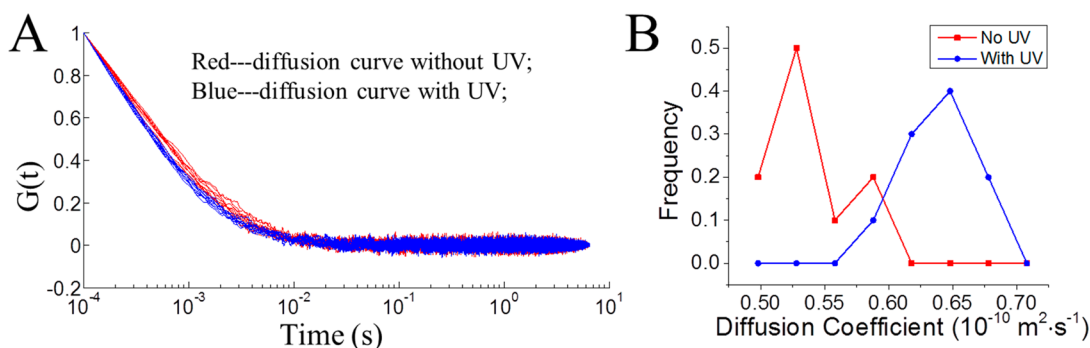


Figure 5. UV light-enhanced diffusion coefficient of USN-1 molecule in a more viscous solvent (ACN:TDE 9:1). (A) The normalized ACFs in the presence and absence of UV light. Red curves: without UV. Blue curves: with UV activation. (B) Recovered diffusion coefficient distributions.

careful design of control molecules with no motor, a slow motor, or a non-unidirectionally rotating motor, we found that a fast unidirectional rotating motor at the MHz range is crucial for increased diffusion, but a non-unidirectional motor can also work, albeit less effectively. No significant change in the diffusion enhancement ratio with increased solvent viscosity was observed. The enhancement of 26% in diffusion suggests that the USN molecules will give ~ 9 nm step upon each motor actuation. While the mechanism of movement is still under study, the activated motion of the molecular-sized entities is possible in spite of Brownian motion in solution. This study provides insight in molecular designs for submersible nanomachines.

Methods. General Synthetic Methods. ^1H NMR and ^{13}C NMR spectra were recorded at 400, 500, or 600 and 100, 125, or 150 MHz, respectively. Chemical shifts (δ) are reported in ppm from tetramethylsilane (TMS). FTIR spectra were recorded using a FTIR infrared microscope with ATR objective with 2 cm^{-1} resolution. All glassware was oven-dried overnight prior to use. Reagent grade tetrahydrofuran (THF) and ether (Et_2O) was distilled from sodium benzophenoneketyl under N_2 atmosphere. Triethylamine (NEt_3), dichloromethane (CH_2Cl_2), and N,N' -dimethylformamide (DMF) were distilled from calcium hydride (CaH_2) under N_2 atmosphere. THF and NEt_3 were degassed with a stream of argon for 15 min before being used in the Sonogashira coupling reactions. All palladium-catalyzed reactions were carried out under argon atmosphere, while other reactions were performed under N_2 unless otherwise noted. All other chemicals were purchased from commercial suppliers and used without further purification. Flash column chromatography was performed using 230–400 mesh silica gel from EM Science. Thin-layer chromatography was performed using glass plates precoated with silica gel 40 F_{254} 0.25 mm layer thickness purchased from EM Science.

UV-vis Measurements. UV-vis spectra were recorded on a Shimadzu UV-2450 or a HP 8543 UV-vis spectrophotometer using spectroscopic grade acetonitrile.

Monitoring of Half Rotation of the Motor. The ^1H NMR spectra of 1 mM solutions of slow motor **32** and USN-3 in CD_3CN were recorded using a Bruker AVANDE III HD 600

MHz High Performance Digital NMR. The samples were excited at 365 nm for 1 h using a UVGL-55 lamp (6 W). The yields of the conversion were calculated using the integration values of the methyl group (Me).

Sample Preparation for Microscopic Measurements. Cy-5 attached-USN molecules were first dissolved in ACN (Fisher Scientific Inc.) as a stock solution with a concentration of $\sim 50 \mu\text{M}$. In single molecule FCS experiments, the solution was serially diluted in ACN to a final concentration of 2.0 nM. The solution was then sandwiched between a piece of Corning no. 1.5 coverglass and a piece of glass slide using two pieces of double-sided Scotch tape ($\sim 90 \mu\text{m}$) as the spacers. Finger nail polish was used to seal the solution in the chamber. To study the viscosity effect on the increased diffusion by UV-light, 2,2'-thiodiethanol (TDE, Sigma-Aldrich) was used to form a binary mixture with ACN at different compositions. All solutions were prepared fresh daily.

Confocal Single Molecule Fluorescence Correlation Spectroscopy with UV Activation. The excitation was provided by an unpolarized 633 nm HeNe laser focused to the diffraction limited spot with an output power of ($\sim 3.0 \text{ MW}/\text{cm}^2$) (Uniphase) unless otherwise specified. The excitation beam was collimated to overfill the back aperture of a microscope objective (Nikon, 100 \times Plan Apo/1.40–0.7 oil-immersed). The fluorescence signal was filtered through a 655 long-pass dichroic mirror and a $684 \pm 24 \text{ nm}$ band-pass filter and imaged into a piece of multimode fiber optics (Thorlabs) and detected by an avalanche photodiode (PerkinElmer, SPCM-AQRH-15-FC). The diameter of the fiber optics was $50 \mu\text{m}$ ($\sim 0.8 \text{ AU}$). A programmable counting board was used for photon counting.

In the UV activation experiments, a gallium indium nitride UV LED emitting at 365 nm was used. The LED emission was filtered using a $350 \pm 25 \text{ nm}$ optical filter and focused by an oil immersion objective (NA 1.4) from the opposite side of the microscope objective. The total power of the UV light was $\sim 10 \text{ mW}$ after optical filter cleaning. The UV spot size was estimated to $\sim 10 \mu\text{m}$. The UV activation and no activation experiments were always collected in pairs using the same solution and at the same collection spot. The sequence of

collection has no observable effect on the diffusion coefficient measurements.

The integration time was 30–100 μs , depending on the diffusion speed of the USN molecules. The acquired data were analyzed using MATLAB and Origin software.

Data Analysis. When a molecule diffuses into the detection volume of a confocal fluorescence microscope, a photon burst will be generated and recorded. A typical fluorescence intensity trace for USN molecules diffusing in ACN is shown in Figure 2. The ACF of the intensity trace follows a 3D model eq 4:³²

$$G(\tau) = \frac{1}{\langle N \rangle} \frac{1}{1 + \tau/\tau_{\text{diff}}} \frac{1}{\sqrt{1 + \tau/S^2\tau_{\text{diff}}^2}} \quad (4)$$

where $\langle N \rangle$ is the average number of emitters in the probe volume; S is the aspect ratio of the probe volume r_z/r_{xy} ; τ_{diff} is the characteristic diffusion time assuming that the emitter has an isotropic diffusion coefficient D , eq 5:

$$\tau_{\text{diff}} = \frac{r_{xy}^2}{4D} \quad (5)$$

where r_{xy} and r_z are the distances from the center to where the emission intensity drops to $1/e^2$ in the lateral and axial directions. The r_{xy} and r_z were estimated to be ~ 300 and ~ 900 nm, respectively. The apparent diffusion coefficient D in the absence and presence of UV activation was obtained through NLLS fitting of the experimentally acquired data.

■ ASSOCIATED CONTENT

Supporting Information

The Supporting Information is available free of charge on the ACS Publications website at DOI: 10.1021/acs.nanolett.5b03764.

Detailed experimental procedures and data (PDF)

Additional spectroscopic data (PDF)

■ AUTHOR INFORMATION

Corresponding Authors

*E-mail: amarti@rice.edu.

*E-mail: tolya@rice.edu.

*E-mail: gufeng_wang@ncsu.edu.

*E-mail: tour@rice.edu.

Notes

The authors declare no competing financial interest.

■ ACKNOWLEDGMENTS

G.W. acknowledges North Carolina State University start-up funds and FRPD Award. A.B.K. acknowledges support from the National Science Foundation (CHE-1360979), the National Institutes of Health (1R01GM094489-01) and the Welch Foundation (C-1559). J.M.T. and A.A.M. acknowledge support from the National Science Foundation (CHE-1007483). The authors thank Prof. Felix Castelleno for his insightful discussions.

■ REFERENCES

- (1) Tour, J. M. *Chem. Mater.* **2014**, *26*, 163–171.
- (2) Alberts, B. *Cell* **1998**, *92*, 291–294.
- (3) Kinbara, K.; Aida, T. *Chem. Rev.* **2005**, *105*, 1377–1400.
- (4) Shirai, Y.; Morin, J. F.; Sasaki, T.; Guerrero, J. M.; Tour, J. M. *Chem. Soc. Rev.* **2006**, *35*, 1043–1055.
- (5) Shirai, Y.; Osgood, A. J.; Zhao, Y.; Yao, Y.; Saudan, L.; Yang, H.; Yu-Huang, C.; Alemany, L. B.; Sasaki, T.; Morin, J.-F.; Guerrero, J. M.; Kelly, K. F.; Tour, J. M. *J. Am. Chem. Soc.* **2006**, *128*, 4854–4864.
- (6) Shirai, Y.; Osgood, A. J.; Zhao, Y. M.; Kelly, K. F.; Tour, J. M. *Nano Lett.* **2005**, *5*, 2330–2334.
- (7) Chiang, P. T.; Mielke, J.; Godoy, J.; Guerrero, J. M.; Alemany, L. B.; Villagómez, C. J.; Saywell, A.; Grill, L.; Tour, J. M. *ACS Nano* **2012**, *6*, 592–597.
- (8) Claytor, K.; Khatua, S.; Guerrero, J. M.; Tour, J. M.; Link, S. J. *Chem. Phys.* **2009**, *130*, 164710.
- (9) Khatua, S.; Guerrero, J. M.; Claytor, K.; Vives, G.; Kolomeisky, A. B.; Tour, J. M.; Link, S. *ACS Nano* **2009**, *3*, 351–356.
- (10) Khatua, S.; Godoy, J.; Tour, J. M.; Link, S. *J. Phys. Chem. Lett.* **2010**, *1*, 3288.
- (11) Vives, G.; Guerrero, J. M.; Godoy, J.; Khatua, S.; Wang, Y.-P.; Kiappes, J. L.; Link, S.; Tour, J. M. *J. Org. Chem.* **2010**, *75*, 6631–6643.
- (12) Chu, P.-L. E.; Wang, L.-Y.; Khatua, S.; Kolomeisky, A. B.; Link, S.; Tour, J. M. *ACS Nano* **2013**, *7* (1), 35–41.
- (13) Fournier-Bidoz, S.; Arsenault, A. C.; Manners, I.; Ozin, G. A. *Chem. Commun.* **2005**, *4*, 441–443.
- (14) Paxton, W. F.; Kistler, K. C.; Olmeda, C. C.; Sen, A.; St. Angelo, S. K.; Cao, Y.; Mallouk, T. E.; Lammert, P. E.; Crespi, V. H. *J. Am. Chem. Soc.* **2004**, *126*, 13424–13431.
- (15) Solovev, A. A.; Mei, Y.; Bermúdez Ureña, E.; Huang, G.; Schmidt, O. G. *Small* **2009**, *5*, 1688–1692.
- (16) Howse, J. R.; Jones, R. A. L.; Ryan, A. J.; Gough, T.; Vafabakhsh, R.; Golestanian, R. *Phys. Rev. Lett.* **2007**, *99*, 048102.
- (17) Pavlick, R. A.; Sengupta, S.; McFadden, T.; Zhang, H.; Sen, A. *Angew. Chem., Int. Ed.* **2011**, *50*, 9374–9377.
- (18) Muddana, H. S.; Sengupta, S.; Mallouk, T.; Sen, A.; Butler, P. J. *J. Am. Chem. Soc.* **2010**, *132*, 2110–2111.
- (19) Sengupta, S.; Dey, K. K.; Muddana, H. S.; Tabouillot, T.; Ibele, M. E.; Butler, P. J.; Sen, A. *J. Am. Chem. Soc.* **2013**, *135*, 1406–1414.
- (20) McDermott, J. J.; Kar, A.; Daher, M.; Klara, S.; Wang, G.; Sen, A.; Velegol, D. *Langmuir* **2012**, *28*, 15491–15497.
- (21) Duan, W.; Ibele, M.; Liu, R.; Sen, A. *Eur. Phys. J. E: Soft Matter Biol. Phys.* **2012**, *35*, 77.
- (22) Hong, Y.; Diaz, M.; Córdova-Figueroa, U. M.; Sen, A. *Adv. Funct. Mater.* **2010**, *20*, 1568–1576.
- (23) Giudicatti, S.; Marz, S. M.; Soler, L.; Madani, A.; Jorgensen, M. R.; Sanchez, S.; Schmidt, O. G. *J. Mater. Chem. C* **2014**, *2*, 5892–5901.
- (24) Pavlick, R. A.; Dey, K. K.; Sirjoosingh, A.; Benesi, A.; Sen, A. *Nanoscale* **2013**, *5*, 1301–1304.
- (25) Godoy, J.; García-López, V.; Wang, L.-Y.; Rondeau-Gagne, S.; Marti, A.; Link, S.; Tour, J. M. *Tetrahedron* **2015**, *71*, 5965–5972.
- (26) Klok, M.; Boyle, N.; Pryce, M. T.; Meetsma, A.; Browne, W. R.; Feringa, B. L. *J. Am. Chem. Soc.* **2008**, *130*, 10484–10485.
- (27) Koumura, N.; Geertsema, E. M.; van Gelder, M. B.; Meetsma, A.; Feringa, B. L. *J. Am. Chem. Soc.* **2002**, *124*, 5037–5051.
- (28) Chen, J.; Kistemaker, J. C.; Robertus, J.; Feringa, B. L. *J. Am. Chem. Soc.* **2014**, *136*, 14924–14932.
- (29) Taylor, G. I. *Proc. R. Soc. London, Ser. A* **1951**, *209*, 447–461.
- (30) Ludwig, W. *Zeit. F. Vergl. Physiol.* **1930**, *13*, 397–504.
- (31) Purcell, E. M. *Am. J. Phys.* **1977**, *45*, 3–11.
- (32) Happel, J.; Brenner, H. *Low Reynolds Number Hydrodynamics*; Prentice-Hall: Englewood Cliffs, NJ, 1965.
- (33) Happel, J.; Brenner, H. *Low Reynolds Number Hydrodynamics*, 2nd ed.; Springer: New York, 1981.
- (34) Nelson, B. J.; Kaliakatsos, I. K.; Abbott, J. J. *Annu. Rev. Biomed. Eng.* **2010**, *12*, 55–85.
- (35) Zhang, L.; Abbott, J. J.; Dong, L.; Peyer, K. E.; Kratochvil, B. E.; Haixin, Z.; Bergeles, C.; Nelson, B. J. *Nano Lett.* **2009**, *9*, 3663–3667.
- (36) Peyer, K. E.; Tottori, S.; Qiu, F.; Zhang, L.; Nelson, B. J. *Chem. - Eur. J.* **2013**, *19*, 28–38.
- (37) Lauga, E.; Powers, T. R. *Rep. Prog. Phys.* **2009**, *72*, 96601–96637.
- (38) Wang, J. *Nanomachines. Fundamentals and Applications*. Wiley-VCH: Weinheim, 2013; pp 13–34.

- (39) Morin, J.-F.; Shirai, Y.; Tour, J. M. *Org. Lett.* **2006**, *8*, 1713–1716.
- (40) Neupane, B.; Chen, F.; Sun, W.; Chiu, D. T.; Wang, G. F. *Rev. Sci. Instrum.* **2013**, *84*, 043701.
- (41) Enderlein, J.; Gregor, I.; Patra, D.; Fitter. *Curr. Pharm. Biotechnol.* **2004**, *5*, 155–161.
- (42) Zhong, Z. M.; Lowry, M.; Wang, G. F.; Geng, L. *Anal. Chem.* **2005**, *77*, 2303–2310.
- (43) Klok, M. Motors for use in Molecular Nanotechnology. *Ph.D. Thesis*, University of Groningen, 2009. <http://dissertations.ub.rug.nl/faculties/science/2009/m.klok/> (accessed October 24, 2015).
- (44) Schönle, A.; Hell, S. W. *Opt. Lett.* **1998**, *23*, 325–327.
- (45) Mukhopadhyay, A.; Zhao, J.; Bae, S. C.; Granick, S. *Rev. Sci. Instrum.* **2003**, *74*, 3067.